MEDICAL ROBOTS

RoboCap: Robotic mucus-clearing capsule for enhanced drug delivery in the gastrointestinal tract

Shriya S. Srinivasan[1,2,3]*, Amro Alshareef[1,2,3], Alexandria V. Hwang[1,2,3], Ziliang Kang[1,2], Johannes Kuosmanen[3], Keiko Ishida[2,3], Joshua Jenkins[3], Sabrina Liu[3], Wiam Abdalla Mohammed Madani[2,3], Jochen Lennerz[4], Alison Hayward[2,3,5], Josh Morimoto[3], Nina Fitzgerald[3], Robert Langer[1,3], Giovanni Traverso[1,2,3]*

Oral drug delivery of proteins is limited by the degradative environment of the gastrointestinal tract and poor absorption, requiring parenteral administration of these drugs. Luminal mucus represents the initial steric and dynamic barrier to absorption. To overcome this barrier, we report the development of the RoboCap, an orally ingestible, robotic drug delivery capsule that locally clears the mucus layer, enhances luminal mixing, and topically deposits the drug payload in the small intestine to enhance drug absorption. RoboCap's mucus-clearing and churning movements are facilitated by an internal motor and by surface features that interact with small intestinal plicae circulares, villi, and mucus. Vancomycin (1.4 kilodaltons of glycopeptide) and insulin (5.8 kilodaltons of peptide) delivery mediated by RoboCap resulted in enhanced bioavailability 20- to 40-fold greater in ex vivo and in vivo swine models when compared with standard oral delivery ($P < 0.05$). Further, insulin delivery via the RoboCap resulted in therapeutic hypoglycemia, supporting its potential to facilitate oral delivery of drugs that are normally precluded by absorption limitations.

INTRODUCTION

Although it is the most common, cost-effective, and practical method of drug administration, oral drug delivery for macromolecules including nucleic acids and proteins is limited by the degradative environment of the gastrointestinal (GI) tract and poor absorption (*1*). Drugs must overcome the harsh acidic environment of the stomach, dissolve in GI fluid, remain stable among dynamic intestinal microbiota and degradative enzymes, penetrate through the viscous mucus barrier, and evade efflux pumps to achieve therapeutic bioavailability (*2*, *3*). Subtherapeutic oral bioavailability levels lead many drugs to require alternate, and often more burdensome, routes of administration. For instance, insulin, required daily for millions of diabetic patients globally, is a peptide with an oral bioavailability of less than 1%, necessitating subcutaneous injections, which can lead to injection-related anxiety, pain, and nonadherence (*4*–*6*). Alternatively, in the case of vancomycin, a small molecule commonly used in serious Gram-positive bacterial infections, an oral bioavailability of 0.069 to 4% forces intravenous administration, requiring costly hospitalization (*7*–*9*). Technologies to overcome the hurdles of absorption, distribution, metabolism, and elimination, which are necessary to allow chemical candidates to mature into drugs, present a major opportunity to help patients receive necessary pharmacological therapy and support the pharmaceutical industry in developing more broadly acceptable drugs (*10*).

Absorption, the first stage of entry, is predominantly hindered by the mucus barrier. Through its viscous, hydrophilic, frequent turnover and shear-thinning gel properties, mucus serves as a dynamic, steric, and interactive barrier, preventing drugs in the lumen from reaching the epithelial surface (*11*). Previously, microstirrers have been developed to perform in situ stirring and have demonstrated the ability to increase absorption rate and bioavailability (*12*). Nanobiotechnology approaches, including tubular micrometers coated with pH-responsive polymers, are capable of targeted delivery and have demonstrated increased retention in gastric tissues and mucosa, but their application is restricted to certain types of drugs and has not been scaled to large animal models or humans (*13*, *14*). Mucus-penetrating PEGylated liposomes have increased tissue permeability, although they require cumbersome drug-specific optimization (*15*). Ultrasound vibrations (*16*) and low-frequency microvibrations (*17*) have also shown efficacy in mechanically inducing higher transport rates but require more convenient administration modes for clinical utility. Drug transport rates across viscous mucus can be accelerated by increasing drug dispersion, inducing mixing in the mucus layer, and by temporarily exposing the epithelial layer.

Here, we describe the development of the RoboCap, an orally ingestible robotic drug delivery device that locally clears the mucus layer, enhances mixing, and topically deposits the drug payload to enhance drug absorption (Movie 1). The RoboCap's rotational and churning movements are generated by surface features designed to interact directly with small intestinal (SI) plicae, villi, and mucus. We hypothesize that drug bioavailability will be significantly greater when delivered with the RoboCap compared with standard oral delivery. We test the efficacy of the RoboCap in delivering two model peptide drugs, vancomycin and insulin, through Franz cell diffusion and in vivo testing in swine.

[1]Department of Mechanical Engineering, Massachusetts Institute of Technology, Cambridge, MA 02139, USA. [2]Division of Gastroenterology, Hepatology and Endoscopy, Brigham and Women's Hospital, Harvard Medical School, Boston, MA 02115, USA. [3]David H. Koch Institute for Integrative Cancer Research, Massachusetts Institute of Technology, Cambridge, MA 02139, USA. [4]Department of Pathology, Massachusetts General Hospital, Boston, MA 02114, USA. [5]Division of Comparative Medicine, Massachusetts Institute of Technology, Cambridge, MA 02139, USA.
*Corresponding author. Email: shriyas@mit.edu (S.S.S.); cgt20@mit.edu, ctraverso@bwh.harvard.edu (G.T.)

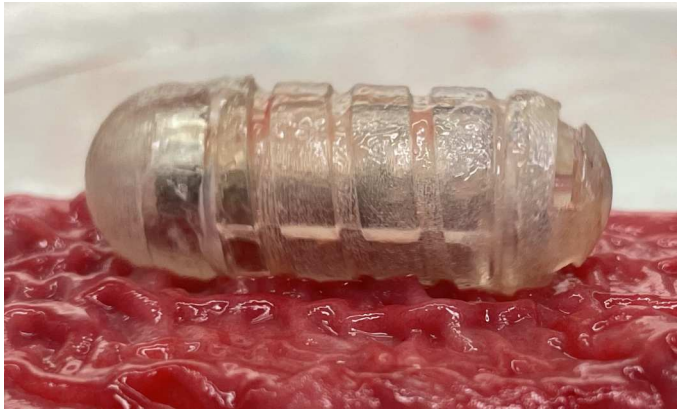

Movie 1. Overview of the RoboCap: The RoboCap is an ingestible capsule that robotically clears intestinal mucus and delivers drugs to heighten absorption and bioavailability.

RESULTS

RoboCap design, function, and interaction with the small intestine

The RoboCap, sized as a triple-zero capsule, is ingestible and carries a drug payload volume of up to 342.6 mm^3 in its cargo hold (purple component in Figs. 1C and 2A). A gelatinous coating hides the surface architecture to prevent abrasion or discomfort during swallowing (Fig. 1A). Then, during passage in the stomach, gastric fluid erodes this gelatinous coating to expose the RoboCap's surface features (Fig. 1A). Upon reaching the small intestine, the pH of the intestinal fluid triggers a dissolvable activation membrane, closing the onboard circuit to start the RoboCap. Internal to the RoboCap, an offset weight laterally mounted on a motor generates a centripetal force, F_c, causing the RoboCap to vibrate and rotate against surface friction, F_{cf},which pulls the RoboCap radially outward and changes its direction theta with the offset motor weight (Fig. 2B and Eq. 1)

$$F_c = m_{weight} * \omega_{weight}^2 * r_{weight} \quad (1)$$

$$f = \frac{\omega_{weight}}{2 * pi} \quad (2)$$

where ω_{weight} is the angular velocity of the motor weight and r_{weight} is the radial offset of the weight from the central axis of the RoboCap. The resulting vibrational frequency of the capsule is f. The oscillatory movement of the capsule is caused by the offset of this force to one side of the capsule by x_w from the center of mass, which causes the capsule to rock back and forth (teeter-totter effect) as the weight moves with and against the force of gravity

$$\sum L = L_{weight} + L_{capsule} = 0 \quad (3)$$

where angular momentum $L_{weight} = I_{weight} * \omega_{weight}$ and $L_{capsule} = I_{capsule} * \omega_{capsule}$

$$I_{weight} * \omega_{weight} = -I_{capsule} * \Omega_{capsule} \; given \;\; \omega_{weight} \gg \Omega_{capsule} \quad (4)$$

The rotational velocity of the capsule is governed by conservation of momentum within the system. In a frictionless environment, because the motor secured within the capsule spins at ω_{weight}, the capsule will counter that spin with an angular velocity $\Omega_{capsule}$, proportional to the rotational rate of the motor and scaled by a ratio of the moment of inertia of the weight, I_{weight}, to that of the capsule, $I_{capsule}$. Detailed analysis of the contribution of gravity and the motor to the RoboCap's motion is provided in note S2.

During its rotation, the RoboCap's surface features mechanically interact with the intestinal plicae, villi, and mucus (Fig. 1, E to H) to enhance drug delivery through various mechanisms. The external helix (1.0 mm) enables optimal contact with the plicae (1 to 10 mm), and the rounded slits (0.5 mm) interface with the villi (0.2 to 8 mm), together facilitating rotation. The contoured surface also maximizes mucosal surface contact wherein microtextured (200- to 300-μm) studs seated on the recessed surfaces churn and clear the 500- to 800-μm-thick mucus layer coating the epithelium (*18*). With each rotation, the drug load erodes away, layer by layer, depositing drug particles. The RoboCap is active for ~35 min and is moved along the tract by peristalsis whereby it is passed by defecation. The RoboCap's design incorporated practical considerations to enable versatile use. For example, the drug payload is positioned at one end of the capsule, allowing it to be easily manipulated by pharmacists who can load any drug of choice. In addition, the RoboCap's pH sensitivity can be tuned to target other segments of the GI tract by modifying the properties of the dissolvable membrane. Fully dimensioned designs of the RoboCap can be found in fig. S8.

Surface property optimization

To optimize rotation, we compared surface geometries incorporating spiral, helical, and studded features with a smooth exterior. Rotation rate was measured as the RoboCap rotated on freshly excised SI tissue. Rotation rate was found to be significantly increased with a helical groove [6.9 ± 1.6 rotations per minute (rpm), $P < 0.01$, two-tailed heteroscedastic t test], likely due to alignment with plicae and accentuation of the oscillatory effect as compared with the smooth exterior (4.2 ± 1.9 rpm).

Spiral extrusions (5.6 ± 1.5 rpm, $P < 0.05$, two-tailed heteroscedastic t test) also significantly enhanced the rotation rate, although studded exteriors did not (2.6 ± 0.9 rpm, $P > 0.05$, two-tailed heteroscedastic t test; Fig. 2, C and D, $n = 20$ trials for each). Thus, an outer body comprising a helical groove was selected for the RoboCap. Rotation rates in air, water, chyme, and mucus were also tested to provide insight on the expected range of rotation rates as the RoboCap encounters diverse media in the small intestine. Rates were significantly different in chyme, water, and mucus as compared with air ($P < 0.05$, two-tailed heteroscedastic t test; Fig. 2E, $n = 5$ trials each). However, less than 30% variability was observed between media, indicating that the RoboCap would function as desired even under the most viscous conditions. Rotation and mixing of viscous mucus (stained red) in luminal fluid (green) can be seen in movie S1.

In the recesses of the helical outer body, studs were fabricated to interrupt beds of mucus as the RoboCap strokes the surface. Studs with heights ranging from 200 to 800 μm were assessed for their capability to wick and remove mucus (Fig. 2F). We compared these against a positive control in which we manually removed mucus using a comb-like device brushed against the tissue 10 times with a constant downward force. A negative control in which no mucus was removed and no RoboCap was placed was also evaluated.

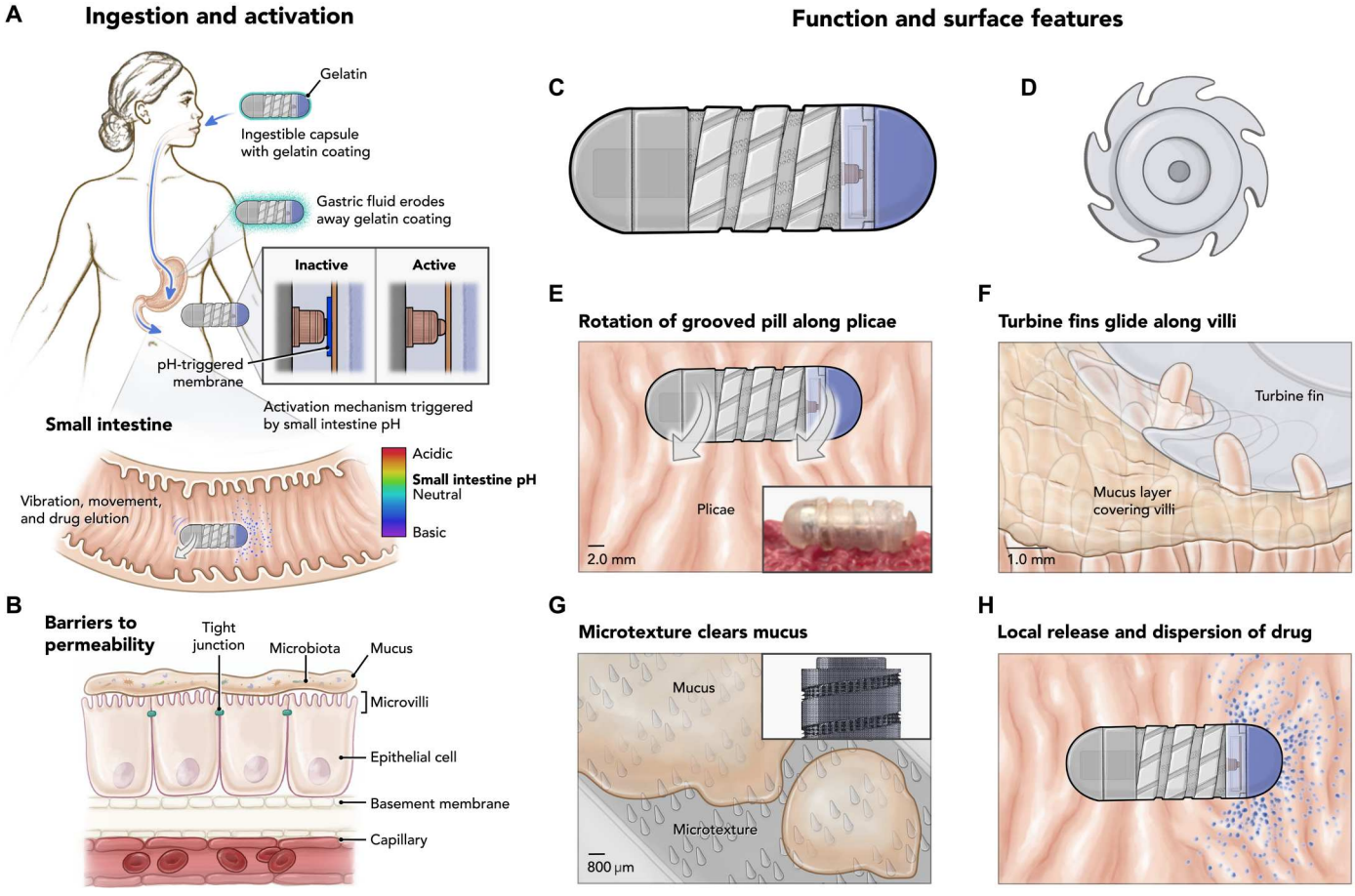

Fig. 1. RoboCap mechanism of action. (**A**) Ingestion process and activation trigger serial dissolution of pH-sensitive gelatinous membranes to expose surface features and close the circuit to activate the RoboCap in the appropriate region of the GI tract. (**B**) Barriers to drug absorption include the mucus, tight junctions, microbiota of the small intestine, and other anatomical features of the tract. (**C**) Side view and (**D**) cross-sectional view of the RoboCap. (**E**) Helical surface grooves enable rotation against SI plicae. (**F**) Fin-shaped cuts enable the pill to glide and scrape mucus from villi. (**G**) Microtexture comprising of an array of studs wicks the mucus. (**H**) Drug loaded into the capsule erodes away, layer by layer, during rotation of the RoboCap onto the luminal surface.

After 20 min of treatment in freshly excised SI tissue, the surface contents of the capsule and luminal fluid were collected using a standardized washing technique (see Materials and Methods). The collected sample was then assessed with absorbance spectroscopy at 330 nm, where higher absorbance indicated a greater concentration of mucus displaced from the SI lining. Studs of all lengths significantly increased mucus removal and presence in the luminal fluid ($P < 0.05$, two-tailed heteroscedastic t test, $n = 9$ trials per condition; Fig. 2, G and H). The 800-μm studs enabled the greatest clearing and wicking of mucus. The effect of stud length was also validated on a Franz cell experiment testing fluorescein isothiocyanate (FITC)–dextran permeabilities. Studs significantly increased permeability as their length increased ($P < 0.05$, two-tailed heteroscedastic t test; fig. S4).

Inspired by torpedo blades, we incorporated rounded slits serving as turbine fins (Fig. 1F) in the helical outer body to generate the propulsion of dislodged mucus into the luminal cavity and enhance mixing of luminal fluids. Videography of this feature evinces greater mixing of viscous mucus (red) in luminal fluid (green) (movie S2).

To quantify the ability of the RoboCap to wick mucus, we performed finite element analysis and assessed the displacement and stress fields of the mucus interacting with the rotating RoboCap (Fig. 2, K to M, and movie S2). Numerical results show that the studded features and grooves wick the mucus more effectively to cause it to turn with the pill as compared with a smooth exterior.

Heightened dispersion and mixing

The RoboCap's mixing capabilities were characterized by imaging a reaction chamber at 0, 5, 10, 20, and 30 min with the drug (blue powder) and RoboCap operating at motor frequencies of 0 (control), 50, 80, and 120 Hz (Fig. 2G). Absorbance measurements of liquid samples from the top, middle, and bottom of the chamber quantitatively indicated that the RoboCap enabled faster dissolution of the drug and greater spatial dispersion when compared with the control (fig. S1A). Motor frequencies of 80 and 120 Hz performed better than 50 Hz. Given the power considerations, 80 Hz was chosen as the operational frequency. After the removal or reduction in mucus at the surface of the intestinal epithelium, this increased dispersion enables a greater number of cells to achieve contact with the drug, thus increasing the probability of uptake through

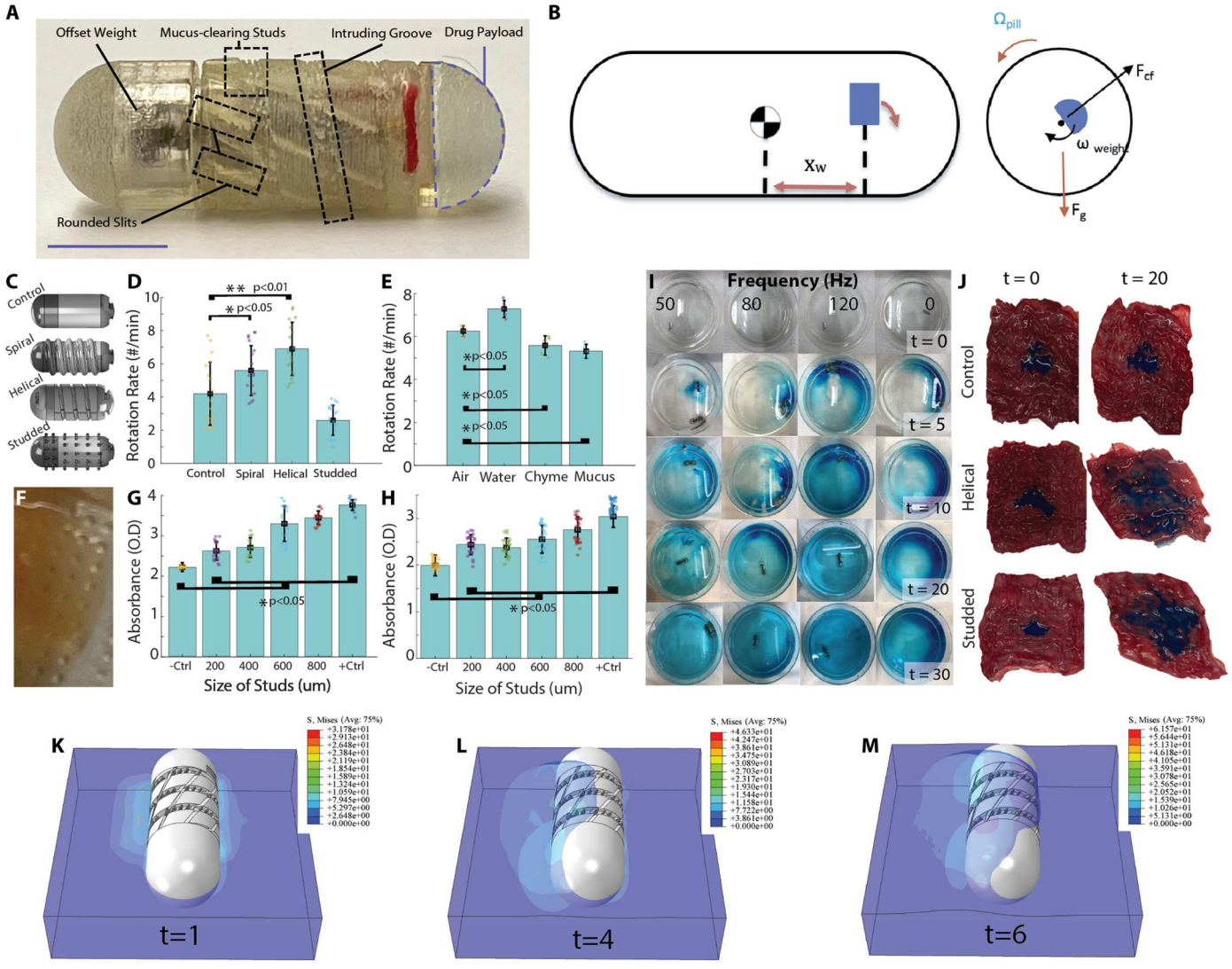

Fig. 2. RoboCap design and optimization. (**A**) RoboCap device with all major components labeled. Scale bar, 6.5 mm. (**B**) Left: A side view of the RoboCap with the center of gravity and offset weight (blue) marked. Right: Cross-sectional view of the RoboCap showing the main forces contributing to the rotational movement. (**C**) Surface geometries to enhance rotation, movement, and churning featured helical grooves, studs, and smooth surfaces. (**D**) Rotation rate on the swine small intestine ex vivo was significantly enhanced for helical and spiral surface geometries as compared with flat or studded controls. (**E**) Rotation rate in various media demonstrates the influence of frictional constraints induced by fluid drag on movement. (**F**) Close-up photograph of mucus adhered to the studs on the surface of the RoboCap. (**G**) Optical absorbance of luminal fluid in a 4-cm segment of the intestine after 30 min of treatment with the RoboCap featuring studs with various heights. (**H**) Optical absorbance quantification of mucus adhered to RoboCaps after 30 min of rotation in the swine small intestine with various stud heights. (**I**) Mixing of drug (blue) in reaction chamber with RoboCap at various frequencies. (**J**) Dispersion of drug (blue dye) after delivery by a sham control, helically grooved RoboCap, or studded RoboCap at $t = 0$ and 20 min. (**K** to **M**) Numerical modeling of the stress field of the mucus adhered to RoboCaps after 6 s of rotation, with a rotation speed of 0.5236 rad/s.

mechanisms of mass transport and potential saturation of mucin fibers (*19*–*22*).

Drug erosion and dispersion on SI tissue surfaces were also assessed using swine SI tissue after 30 min of RoboCap activity. The drug was dispersed over a greater surface area when delivered with RoboCap as compared with the control ($P < 0.05$) (Fig. 2H). With surface features and motor frequency optimized for mixing, dispersion, and clearing of mucus, we performed a range of ex vivo and in vivo studies to quantify the efficacy of the RoboCap in enhancing drug absorption. Using a Franz cell apparatus, vancomycin was delivered to the donor well either by direct dilution in the donor well or with the RoboCap.

Various surface geometries were tested across 25 independent tissue samples derived from $n = 5$ animals. Given the interanimal variability of tissue properties, a ratio of permeability induced by the RoboCap to the control condition within the same animal was calculated. Vancomycin drug permeability was observed to increase more than 10-fold with RoboCap delivery (either flat or helical surfaces) as compared with controls ($P < 0.05$; Fig. 3A). Furthermore, those with helical surface geometries significantly outperformed those with flat surface geometries ($P < 0.05$) (Fig. 3B).

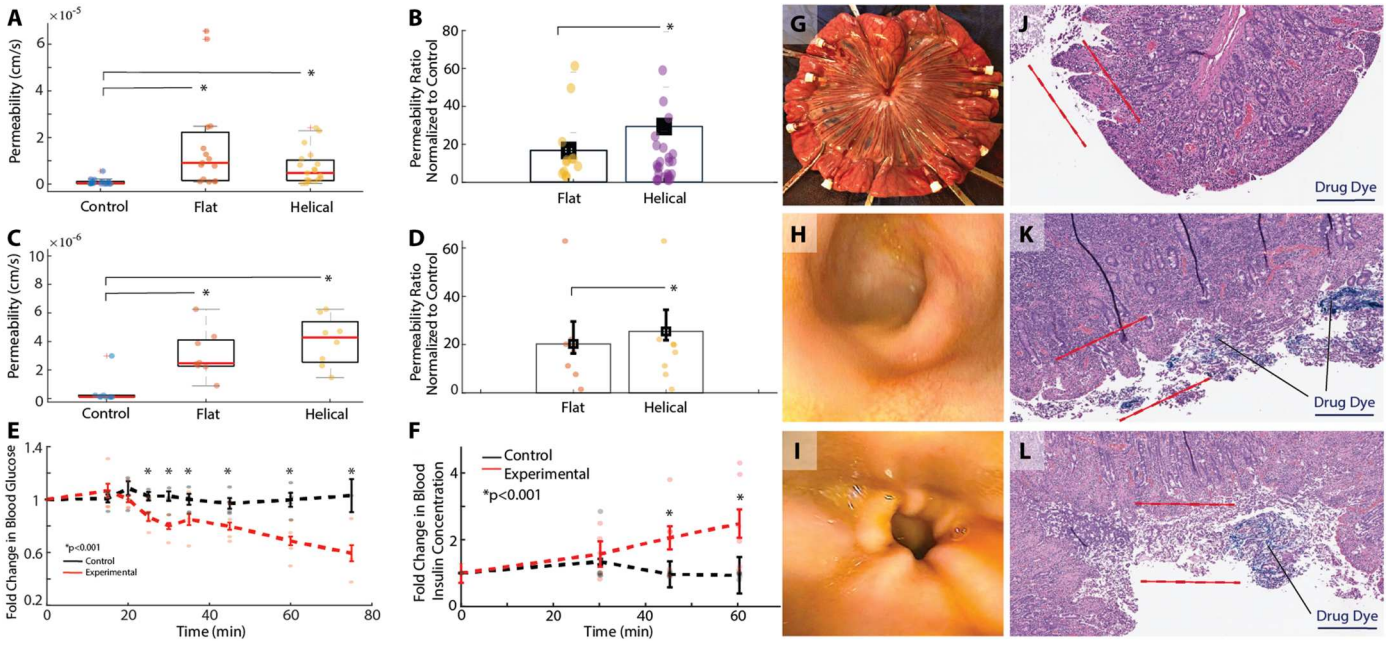

Fig. 3. In vivo RoboCap function. (**A**) Drug permeabilities for vancomycin when delivered with a sham pill (control) or RoboCap with flat or helical surface geometries in a Franz cell apparatus on the SI swine tissue. (**B**) Permeabilities are normalized to the control group and demonstrate a greater than 10-fold increase in efficacy when drug is delivered with a RoboCap. (**C**) Drug permeability in the swine small intestine in vivo for vancomycin delivery by sham (control) pills or a helical or flat RoboCap. (**D**) Permeabilities are normalized to their matched pair in the control group, demonstrating more than 20-fold improvements when drug is delivered with a RoboCap. (**E**) Blood glucose and (**F**) blood insulin concentrations in swine after insulin delivery by endoscopic luminal spray (control, black) or via RoboCap (experimental, red). (**G**) Isolation of independent SI sections for permeability testing. Endoscopic appearance of the small intestine (**H**) before and (**I**) after treatment with a RoboCap. Hematoxylin and eosin staining of cross sections of the small intestine after treatment with a blue-dyed drug to assess permeation in (**J**) control and (**K** and **L**) RoboCap-treated cases. Red lines indicate the region of microvilli, brush border, and mucus residence. Indicator lines point to representative areas of dye deposition. Scale bars, 4 mm. Box plots represent quartiles, and dots represent individual measurements.

A chemical resistance test was performed to evaluate the chemical stability of the RoboCap. RoboCaps (n = 5) with disabled activation mechanisms were immersed in simulated gastric fluid or simulated intestinal fluid for 72 hours at 37°C. Upon removal, 100% of the capsules were able to be activated and functioned normally (fig. S6). In addition, 10 capsules were placed in the small intestine of a swine for at least 60 min. After removal, 10 of 10 capsules functioned normally when tested on the benchtop. No significant difference was observed in the rotation rate of RoboCaps between those that were exposed to the small intestine and air (control) ($P > 0.05$, two-tailed heteroscedastic t test; fig. S6). Furthermore, to evaluate potential thermal risks, we continuously operated the RoboCap in a volume of 10 ml of simulated intestinal fluid. The temperature over the course of a 30-min period shifted less than 1°C, posing no thermal risk for the SI tissue.

In vivo study

To assess the efficacy of the RoboCap in facilitating peptide drug delivery, we used the model peptide drugs vancomycin and insulin. In an anesthetized swine, sections of the small intestine were first isolated to serve as independent testing sites while controlling for animal-specific properties such as hydration status, peristaltic rate, blood pressure, and perfusion (Fig. 3G). RoboCaps or sham pills carrying 100 mg of vancomycin were placed into each section. Then, vancomycin permeability was assessed through venous blood collection from the mesenteric plexus stemming from each section. Consistent with the Franz cell studies, RoboCaps resulted in significantly higher tissue permeabilities, greater than 20 times that of the control ($P < 0.001$; Fig. 3C). The helical surface additionally demonstrated a significant advantage over the smooth exterior when normalized to control samples ($P < 0.001$; Fig. 3D). Furthermore, vancomycin concentration significantly increased in the venous mesenteric blood supply over a 60-min period when delivered with a RoboCap ($P < 0.01$), whereas control samples saw no trend (fig. S2A).

Furthermore, we delivered insulin (100 U) via the RoboCap (n = 7 animals, experimental) and compared it with an endoscopic spray in the small intestine (control, n = 5). Blood glucose and insulin concentrations were monitored for a 75-min period with the drug delivery starting at 15 min. The RoboCap significantly increased the bioavailability of insulin, causing a sharp decrease in blood glucose levels ($P < 0.001$; Fig. 3E) and an increase in blood insulin levels ($P < 0.001$, n = 5 animals; Fig. 3F) when compared with controls (n = 5). Animals treated with the RoboCap demonstrated an average blood glucose reduction of 55.54 ± 16.1 mg/dl, whereas controls demonstrated a variance of 16.6 ± 17.3 mg/dl from baseline. Observed tissue permeabilities were more than twofold greater than the previously reported permeabilities of insulin (*23*). These results are in a range similar to those of other strategies involving microneedles that circumvent the mucus barrier. When animals were treated with the RoboCap, changes in blood glucose levels were seen within 15 min and continued through the end of the monitoring period. In three animals, hypoglycemia (blood glucose < 20 mg/dl) ensued at 60 min, necessitating

dextrose infusion. These indicated a steady and significantly enhanced drug absorption rate that makes oral insulin delivery viable for therapeutic applications via the RoboCap.

To visualize drug permeation in the tissue, we encapsulated a blue dye in the RoboCap and administered it to SI tissues ex vivo. After 30 min of treatment, tissues were fixed, paraffin-processed, and stained with hematoxylin and eosin. Blue particulates can be visualized permeating more deeply into the microvilli and epithelial layers in tissues treated with RoboCaps (Fig. 3, K and L, and fig. S2) as compared with orally administered controls (Fig. 3J and fig. S2). These visualizations reinforce the mechanism of the RoboCap clearing mucus and locally depositing drug for epithelial uptake.

After oral or endoscopic delivery to the small intestine, RoboCaps safely transited through the GI tract of the animal without complications, perforation, or obstruction in 10 of 10 trials. No erosion of the mucosa, inflammation, infection, or hematological complications were sustained, as observed by endoscopy (Fig. 3, H and I) performed before and after RoboCap activity. Using radiography, we monitored the RoboCap passing through the animal alongside radiopaque (barium sulfate) beads, which serve as a proxy for motility rate (fig. S3). Controls treated with a sham pill and those treated with RoboCap passed the beads in 7.6 ± 2.7 and 6.3 ± 1.9 days. No significant difference in the rates of passage was observed at an alpha value of 0.05 (fig. S3).

Histological analysis was performed on cross-sectional samples from control (n = 9) and RoboCap-treated (n = 16) samples (table S1) by a blinded pathologist. The epithelium, surface brush border, inflammation of the epithelium, and surface lamina propia were assessed on hematoxylin and eosin– and trichrome-stained cross sections to assay for damages to the epithelium caused by the RoboCap′s erosion of mucus. No significant differences in any category were assessed, as per two-tailed heteroscedastic t tests. Furthermore, there was no significant difference in the levels of edema (control = 1 ± 0.707, stimulated = 0.93 ± 0.25) and inflammation (control = 1.33 ± 0.866, experimental = 1.31 ± 0.47) between groups ($P > 0.1$). These data support the safety of the RoboCap and its easy passage through the GI tract. Macromolecular uptake is mediated by absorptive villous epithelial cells, including previously described vacuolization (*20*–*22*), which can be regarded as a morphological indicator of absorptive activity. No control samples demonstrated a remarkable degree of vacuolization; however, 6 of 16 experimental samples exhibited pronounced vacuolization, indicative of enhanced uptake behavior related to RoboCap activity (*20*–*22*).

To assay the capability of the RoboCap to assist in the delivery of larger molecules, we delivered FITC-dextran of various molecular weights using the RoboCap, at various motor frequencies, and compared with direct application (controls). The RoboCap was able to significantly increase uptake even with molecular weights as high as 150 kDa, although the greatest increases were seen at 40 and 70 kDa (fig. S4). The frequency of the internal motor did not have a measurable effect on the rate of uptake.

DISCUSSION

This study demonstrates the utility of the RoboCap in enhancing oral drug absorption through localized drug delivery, increased drug dispersion, and mucus-clearing mechanisms. Both ex vivo and in vivo testing consistently demonstrated a greater than 10-fold increase in drug permeability for small-molecule and peptide drug models. Insulin delivery using the RoboCap resulted in a more gradual uptake as compared with the pharmacodynamics of subcutaneous or intravascular injection, which may be a useful feature for various drugs requiring gradual or sustained release. RoboCap insulin delivery further resulted in a decrease of blood glucose levels in all animals and even caused unanticipated and supratherapeutic hypoglycemia in three of seven animals. This substantiates its significant potential to enable oral delivery of molecules that have previously seen little success by oral administration. Future studies in swine and humans should optimize the dosage for such drugs to identify the therapeutic ranges via SI delivery. Increasing the efficacy of orally administered drugs with poor availability can, in turn, limit dosages and thereby increase safety, compliance, and convenience and reduce cost.

Unlike other drug carrier systems, such as lipid-based formulations or nanoparticles, the RoboCap yields no biocompatibility concerns, because the electromechanical components remain sealed off and pass through the body after the drug is delivered (*24*). The mucus barrier serves to protect against pathogens; hence, excessive mucus clearing could pose an infectious risk. However, frequent turnover and constant production of mucus prevent the RoboCap from excessively depleting the mucus. This can be benchmarked against more severe interventions that deplete the mucus barrier, such as polypectomies, where side effects of infection are extremely rare (<0.2%) (*25*).

Capsule design can be further enhanced to improve RoboCap function and expand its utility to other applications. For instance, geometries that reduce the contact surface area or surface friction on the capsule-fluid boundary would result in an increased rotation rate of the RoboCap. In addition, varying the material or geometry of the offset weight could increase the capsule′s inertia, resulting in an increased rotation rate. A relative rotation mechanism, where the two sides of the RoboCap rotate in opposite directions, could enable increased mixing of the surrounding fluid. Given the RoboCap′s ability to rotate and create mixing, it can be adapted for the in situ generation of topical/intraluminal foams, which currently require endoscopic application (*26*). RoboCaps may also assist in topical administration of therapeutics, including mesalamine and corticosteroids.

Clinical translation will be facilitated by design iterations to miniaturize components and safety and efficacy validations. On the basis of considerations including the chemical stability and safety of the drug, formulation media, and costs associated with manufacturing and scaling drug-specific capsules, RoboCap may be loaded with the desired drug during manufacturing or pharmaceutical preparation for personalized dosing. The presence of metal within the pill could make RoboCap difficult to use in patients who require imaging techniques involving magnets, such as magnetic resonance imaging. However, other ingestible devices such as the PillCam have overcome this limitation, and such techniques could be adapted for this capsule. Furthermore, the current design incorporates rigid batteries to provide adequate motor power (~250 mW). As wireless, battery-free, and energy-harvesting systems advance, they could potentially be incorporated to eliminate rigid electronics inside the RoboCap. The material components of the RoboCap are similar to those of Food and Drug Administration–approved ingestible devices, such as osmotic-controlled release oral delivery (OROS) capsules, ingestible temperature sensors, and capsule endoscopy

systems, yielding comparable environmental considerations (*27*, *28*). Systems to retrieve the RoboCaps from excreted waste must be considered to minimize the potential environmental complications of disposing such components into the common sewage systems.

In conclusion, as an ingestible robotic capsule, the RoboCap effectively clears mucus, enhances mixing, and topically deposits a drug payload, leading to significantly improved drug absorption. As we demonstrated in the case of insulin delivery, the RoboCap makes it possible to achieve therapeutic absorption levels through oral ingestion for drugs that usually require more cumbersome and expensive methods such as subcutaneous injections, inhalers, and intravenous administration, requiring hospitalization.

MATERIALS AND METHODS

Design of the RoboCap

The RoboCap was designed using SolidWorks. Its framework was based on a triple-zero capsule's dimensions to aid oral administration. A central compartment houses the battery, resistor, motor (1.5 V, 3 V, 6 mm–by–10 mm miniature microvibrating coreless motor, A00000308), and offset weight. The circuitry in this compartment is closed upon dissolution of a polymer membrane that degrades at the pH of SI fluid. This allows the pogo pin attached to the battery to contact the motor lead, thus closing the circuit. A secondary compartment houses the drug load and can be press-fit onto the main compartment. A 1.55-V, 80-mA·hour silver oxide battery (DigiKey) was used because of its biocompatibility and its high capacity-to-size ratio. Prototypes were three-dimensionally (3D) printed (Stratasys) using the VeroClear photopolymer, which was selected for its biocompatibility, chemical resistance, and transparency. Capsules were thoroughly cleaned with water and ethanol before administration. In preparation for assembly, the 3D printed parts were submerged in a 2% sodium hydroxide solution and stirred for 15 min. The parts were then rinsed four times in deionized water before being left to dry. Detailed assembly information is provided in note S1.

Motor frequency was modulated through the use of resistors (DigiKey), ranging from 0 to 120 ohms, placed between the battery and the motor (fig. S7). The frequency of vibration was verified using a tachometer to measure the rotation rate of the offset weight over the period of 10 s. An inverse relationship was observed between the resistance in the circuit and the output operating frequency of the RoboCap.

Various surface geometries were designed and tested on the RoboCap to optimize rotation and mucosal disruption. The baseline geometry used a smooth exterior shell similar to that of standard triple-zero drug capsules. Grooved and protruding spiral geometries were then added to enhance the rotation rate of the RoboCap, taking inspiration from rotating screw mechanisms. Studded arrays along the spirals were incorporated to increase the churning effect on the SI mucosal layer and to further stimulate the villi for drug absorption. Because of the modular nature of the RoboCap, these features were easily incorporated and combined for fast prototyping of various geometries.

To coat RoboCap capsules with gelatin to prevent activation before reaching the small intestine, we placed a 35% (w/v) solution of gelatin (Sigma-Aldrich) in a large petri dish at room temperature. Capsules were then submerged in the solution for about 1.2 hours until the desired thickness of the layer was achieved. After removal, the capsule was gently rotated several times to ensure even distribution around the surface of the pill and then left to set and dry at room temperature in a vented but covered dish. To load a drug into the capsule, we measured a powdered formulation of the desired drug at the appropriate dosage using a balance. A thin spatula was then used to scoop and pack the powder into the RoboCap's drug compartment. This was then sealed and coated with Eudragit-L, which dissolves at pH 6, in the small intestine.

Tissue and in vivo experiments

All animal experiments were conducted in accordance with protocols approved by the Committee on Animal Care at the Massachusetts Institute of Technology, in a swine model [0- to 80-kg Yorkshire pigs (*Sus scrofa domesticus*) ranging between 4 and 6 months of age]. The swine model was chosen because its gastric anatomy is similar to that of humans and has been widely used in the evaluation of biomedical GI devices (*29*). For bench tests assessing mixing and dispersion, mucus was collected from the swine small intestine through the working channel of an endoscope. For all ex vivo studies, intestinal dissection was performed within 10 min of euthanasia, and tissues were maintained in Krebs buffer during transport. The small intestine (100 cm) starting at the duodenum was used for all experiments, prioritizing proximal tissue whenever possible to maintain consistency across experiments.

Characterization of rotation rate

To characterize the rotation rate among various capsule shapes, we marked RoboCaps axially, and rotations were counted for 10 min in a 500-ml reaction chamber. For one set of trials, the reaction chamber was filled with distilled water. For a second set of trials, freshly harvested SI tissue was transected longitudinally and laid flat in the chamber. The RoboCap was placed on top of a thick layer of mucus and observed.

Optimization of surface features

To optimize surface features, we observed the RoboCap operating on freshly harvested tissue. Studs ranging from 200 to 800 μm were evaluated for their ability to clear mucus. After 20 rotations of the capsule in a single location, mucus that adhered to the tissue and to the RoboCap was collected using three washes of 5 ml of distilled water. The absorbance of the solution at 330 nm was recorded at nine points in each of the samples with mixing just before recording. This was performed in triplicate for each sample. A higher absorbance reading indicates a greater concentration of mucus in the sample, representing lesser adherent mucus on the small intestinal surface.

Characterization of dispersion and mixing

Gelatin capsules filled with methylene blue were placed in a reaction chamber filled with distilled water along with the RoboCap operating at various frequencies. At each time point, 2 ml of fluid was sampled from the bottom, middle, and top of the 500-ml chamber. Absorbance spectroscopy at 435 nm was performed to assess the concentration of the drug in the sample. Each sample was measured in triplicate.

The drug chamber of the RoboCap or sham pill was filled with a blue tissue-marking dye to simulate a drug. A helical RoboCap,

studded RoboCap, or sham pill was placed in 3-cm-long isolated segments of the small intestine. After 20 min of operation, the tissue was filleted open and photographed to measure dispersion.

Simulation of rotation and wicking of mucus

Finite element analysis was conducted to characterize the interaction between the mucus and the RoboCap, via the commercial finite element software Abaqus 2021 (SIMULIA). The RoboCap was treated as a polypropylene rigid body, with a density of 900 kg/m^3, a Young's modulus of 1340 MPa, and a Poisson ratio of 0.39. Mucus was modeled as a non-Newtonian fluid under laminar flow, with a density of 1500 kg/m^3. We used the Carreau-Yasuda model to describe the non-Newtonian shear-thinning behavior of the model, where the viscosity μ follows the formula

$$mu = mu_\infty + (\mu_0 - \mu_\infty)(1 + (lambda\dot{\gamma})^2)\frac{n-1}{2} \quad (5)$$

Here, $\dot{\gamma}$ is the shear rate, and the model properties are defined in Table 1.

The simulation space was set at 40 mm (L) by 40 mm (W) by 20 mm (H), where the RoboCap rotates in the center of the cube space. The volume of the mucus was constrained to be half of the space, and initially, the bottom half of the RoboCap was immersed in the mucus. Gravity of 9.81 m/s^2 was applied to the mucus and the RoboCap. The interaction type between the RoboCap and the mucus was set to "hard" for the normal behavior, with a friction coefficient of 0.02 for the tangential behavior. The dynamic explicit solver was implemented to simulate the first 12 s of interaction once the RoboCap started rotating, with an angular velocity of 0.5236 rad/s.

Chemical resistance test

The robustness of the mechanical design and encased electronics were measured by immersing the RoboCaps in simulated gastric or intestinal fluid at 37°C. A small wax plug sealed the inlet to protect the pH-sensitive activation membrane. After 72 hours, the RoboCaps were visually inspected for any mechanical damage. The wax plug was removed, and the capsules were placed in a 50-ml beaker of simulated intestinal fluid and observed for activation.

Thermal testing

To evaluate the thermal safety of the pill, we placed the RoboCap in a 10-ml vial of simulated intestinal fluid and monitored the temperature of the fluid over a 30-min period using a digital thermometer.

Table 1. Non-Newtonian mucus properties for the Carreau-Yasuda model.

Property	Value
Shear viscosity at low shear rates μ_0	0.03
Shear viscosity at high shear rates μ_∞	0.01
Time constant λ	25
Flow behavior index n	0.25

In vitro tissue permeability

To test the RoboCap's function and quantify tissue permeability, we used a Franz cell apparatus as previously described (*23*) with full-thickness intestinal tissue surgically harvested from Yorkshire pigs. Tissue was filleted into rectangular strips, washed with 30 ml of saline to remove food contents, and placed between two magnetic compression plates to create an array of donor and receiver wells. Clear plastic film (Thermo Fisher Scientific) was used to seal the bottom plate, creating a receiver well. The receiver wells were filled with phosphate-buffered saline (PBS; Thermo Fisher Scientific) and 2% bovine serum albumin (Sigma-Aldrich). The donor well was filled with PBS (1×) along with the drug. Vancomycin hydrochloride (Sigma-Aldrich) was dosed at 1000 to 3000 μg/ml. Insulin was dosed at 500 to 2000 μg/ml. In the stimulation group, RoboCaps were placed in the wells of the plate for 30 min. After treatment, internal standards were added to the receiver wells. For vancomycin and insulin experiments, we treated with bleomycin (1 μg/ml) and liraglutide (1 μg/ml) as internal standards, respectively. Then, the contents of the receiver wells were extracted with a 20-gauge needle. Tissues were maintained at 37°C and in Krebs buffer during processing to maximize viability. All tissues were used within 1 hour from the time of harvest. An internal standard was used to determine the losses due to processing or remove wells in which leaks occurred and correct for intertissue variance.. The vancomycin or insulin signals in high-performance liquid chromatography (HPLC) or liquid chromatography–mass spectrometry are normalized to the signals of the respective internal standards to get a relative response and improve precision.

In vivo drug delivery study

To measure the efficacy of RoboCap as compared with traditional pill dissolution and drug uptake, we isolated 4-inch sections of the small intestine after laparotomy in an anesthetized pig (Fig. 3G). Veins in the myenteric plexus were catheterized. Blood was sampled every 15 min during a 45-min treatment period. In each intestinal section, which was separated from the adjacent section by a clamped-off section of the small intestine at least 6 inches long, the RoboCaps or a drug in liquid form was administered. Every other section was kept blank and untreated as a buffer segment to prevent cross contamination and/or leaks. Tissue was kept at physiologic temperatures using warm towels with saline. Blood was centrifuged at 4°C for 15 min. Protease inhibitor (Sigma-Aldrich) was added to the plasma and stored at 4°C for further analysis.

In anesthetized pigs, RoboCaps loaded with insulin were endoscopically delivered to the small intestine. Blood glucose levels were assessed every 5 to 10 min. Blood was collected using an ear vein catheter and processed as described above. The RoboCap's rotation and vibration rates were measured.

All samples were combined with acetonitrile in a 1:3 ratio (v/v) and then centrifuged at 1200 rpm at 4°C for 15 min for protein precipitation and extraction. The supernatant of each tube was then loaded into microtubes and processed using HPLC to quantify the drug concentrations. Vancomycin concentration was analyzed using an Agilent 1260 Infinity II HPLC equipped with a quaternary pump, autosampler, thermostatted column compartment, and ultraviolet diode array detector (DAD). Output signal data processing was performed using ChemStation software. Chromatographic separation was performed using an Agilent Zorbax XDB C18, 4.6 mm

by 150 mm analytical column with a spherical particle size of 5 μm. Separations were performed at a temperature of 50°C. The optimized mobile phase consisted of 0.1% formic acid in water (A) and acetonitrile (B). The gradient elution began at 100% A and 0% B, increasing to 5% A and 95% B over 3 min. The total run time was 5 min with a reequilibration time of 2 min. The flow rate was 0.75 ml/min, and the injection volume was 10 μl. The DAD parameters were as follows: absorbance measured at a wavelength of 280 nm, bandwidth of 4.0 nm, and scan rate of 5 Hz. Standard curves were prepared using fresh vancomycin or insulin to calculate concentrations (fig. S5).

Permeability was calculated with the following formula as per prior reports (*23*)

$$P = \frac{V}{A \times C_0} \times \frac{\Delta C_R}{\Delta t} \quad (6)$$

where V is the volume in the receiver chamber, A is the tissue surface area, C_0 is the initial concentration in the donor chamber, and ΔC_R is the concentration increase in the receiver chamber in the incubation time Δt.

Histology

After euthanasia, SI tissue sections were carefully harvested from animals in the control and experimental groups. Tissues were fixed in 4% paraformaldehyde for 24 hours, washed three times in PBS for 15 min each, and stored in 70% ethanol. Samples were then paraffin-processed, embedded, and sectioned (5 μm). Tissues were stained with hematoxylin and eosin to assess morphology and surveil for adverse side effects related to the intervention. Tissue samples were evaluated by a blinded clinical pathologist for edema, basement membrane disruptions, inflammation, vacuolization, and the presence of goblet cells as per the scales indicated in table S1.

Statistical analyses

Quantitative data are reported as means (±SD) or as a range when appropriate. The normality of the distributions was checked by the Shapiro-Wilk test. Comparative analyses were performed using student's heteroscedastic two-tailed t test unless otherwise noted. $P < 0.05$ was considered significant.

Supplementary Materials

This PDF file includes:
Supplementary Text
Figs. S1 to S12
Tables S1 and S2

Other Supplementary Material for this manuscript includes the following:
MDAR Reproducibility Checklist
Movies S1 to S3

REFERENCES AND NOTES

1. P.-A. Billat, E. Roger, S. Faure, F. Lagarce, Models for drug absorption from the small intestine: Where are we and where are we going? *Drug Discov. Today* **22**, 761–775 (2017).
2. A. Paul, in *Introduction to Basics of Pharmacology and Toxicology: Volume 1: General and Molecular Pharmacology: Principles of Drug Action*, G. M. Raj, R. Raveendran, Eds. (Springer, 2019), pp. 81–88.
3. M. Vertzoni, P. Augustijns, M. Grimm, M. Koziolek, G. Lemmens, N. Parrott, C. Pentafragka, C. Reppas, J. Rubbens, J. Van Den Abeele, T. Vanuytsel, W. Weitschies, C. G. Wilson, Impact of regional differences along the gastrointestinal tract of healthy adults on oral drug absorption: An UNGAP review. *Eur. J. Pharm. Sci.* **134**, 153–175 (2019).
4. R. Aronson, The role of comfort and discomfort in insulin therapy. *Diabetes Technol. Ther.* **14**, 741–747 (2012).
5. D. Kaklotar, P. Agrawal, A. Abdulla, R. P. Singh, Sonali, A. K. Mehata, S. Singh, B. Mishra, B. L. Pandey, A. Trigunayat, M. S. Muthu, Transition from passive to active targeting of oral insulin nanomedicines: Enhancement in bioavailability and glycemic control in diabetes. *Nanomedicine* **11**, 1465–1486 (2016).
6. A. Banerjee, K. Ibsen, T. Brown, R. Chen, C. Agatemor, S. Mitragotri, Ionic liquids for oral insulin delivery. *Proc. Natl. Acad. Sci. U.S.A.* **115**, 7296–7301 (2018).
7. M. Sauter, P. Uhl, A. D. Meid, G. Mikus, J. Burhenne, W. E. Haefeli, New insights into the pharmacokinetics of vancomycin after oral and intravenous administration: An investigation in beagle dogs. *J. Pharm. Sci.* **109**, 2090–2094 (2020).
8. N. Shibata, M. Ishida, Y. Venkata Rama Prasad, W. Gao, Y. Yoshikawa, K. Takada, Highly sensitive quantification of vancomycin in plasma samples using liquid chromatography–tandem mass spectrometry and oral bioavailability in rats. *J. Chromatogr. B* **789**, 211–218 (2003).
9. R. S. Geary, H. Wade Schlameus, Vancomycin and insulin used as models for oral delivery of peptides. *J. Control. Release* **23**, 65–74 (1993).
10. J. Hodgson, ADMET—Turning chemicals into drugs. *Nat. Biotechnol.* **19**, 722–726 (2001).
11. M. Boegh, H. M. Nielsen, Mucus as a barrier to drug delivery—Understanding and mimicking the barrier properties. *Basic Clin. Pharmacol. Toxicol.* **116**, 179–186 (2015).
12. R. Mundaca-Uribe, E. Karshalev, B. Esteban-Fernández de Ávila, X. Wei, B. Nguyen, I. Litvan, R. H. Fang, L. Zhang, J. Wang, A microstirring pill enhances bioavailability of orally administered drugs. *Adv. Sci.* **8**, 2100389 (2021).
13. J. Li, S. Thamphiwatana, W. Liu, B. E.-F. de Ávila, P. Angsantikul, E. Sandraz, J. Wang, T. Xu, F. Soto, V. Ramez, X. Wang, W. Gao, L. Zhang, J. Wang, Enteric micromotor can selectively position and spontaneously propel in the gastrointestinal tract. *ACS Nano* **10**, 9536–9542 (2016).
14. T. Maric, S. Atladóttir, L. H. E. Thamdrup, O. Ilchenko, M. Ghavami, A. Boisen, Self-propelled Janus micromotors for pH-responsive release of small molecule drug. *Appl. Mater. Today* **27**, 101418 (2022).
15. E. Yamazoe, J.-Y. Fang, K. Tahara, Oral mucus-penetrating PEGylated liposomes to improve drug absorption: Differences in the interaction mechanisms of a mucoadhesive liposome. *Int. J. Pharm.* **593**, 120148 (2021).
16. C. M. Schoellhammer, A. Schroeder, R. Maa, G. Y. Lauwers, A. Swiston, M. Zervas, R. Barman, A. M. DiCiccio, W. R. Brugge, D. G. Anderson, D. Blankschtein, R. Langer, G. Traverso, Ultrasound-mediated gastrointestinal drug delivery. *Sci. Transl. Med.* **7**, 310ra168 (2015).
17. S. M. Flaherty, I. J. Russell, A. N. Lukashkin, Drug distribution along the cochlea is strongly enhanced by low-frequency round window micro vibrations. *Drug Deliv.* **28**, 1312–1320 (2021).
18. A. Swidsinski, V. Loening-Baucke, F. Theissig, H. Engelhardt, S. Bengmark, S. Koch, H. Lochs, Y. Dörffel, Comparative study of the intestinal mucus barrier in normal and inflamed colon. *Gut* **56**, 343–350 (2007).
19. A. Schittny, J. Huwyler, M. Puchkov, Mechanisms of increased bioavailability through amorphous solid dispersions: A review. *Drug Deliv.* **27**, 110–127 (2019).
20. Z. Luo, N. Paunović, J.-C. Leroux, Physical methods for enhancing drug absorption from the gastrointestinal tract. *Adv. Drug Deliv. Rev.* **175**, 113814 (2021).
21. S. Gupta, R. Kesarla, A. Omri, Formulation strategies to improve the bioavailability of poorly absorbed drugs with special emphasis on self-emulsifying systems. *ISRN Pharm.* **2013**, e848043 (2013).
22. S. K. Lai, Y.-Y. Wang, J. Hanes, Mucus-penetrating nanoparticles for drug and gene delivery to mucosal tissues. *Adv. Drug Deliv. Rev.* **61**, 158–171 (2009).
23. T. von Erlach, S. Saxton, Y. Shi, D. Minahan, D. Reker, F. Javid, Y.-A. L. Lee, C. Schoellhammer, T. Esfandiary, C. Cleveland, L. Booth, J. Lin, H. Levy, S. Blackburn, A. Hayward, R. Langer, G. Traverso, Robotically handled whole-tissue culture system for the screening of oral drug formulations. *Nat. Biomed. Eng.* **4**, 544–559 (2020).
24. M. S. Alqahtani, M. Kazi, M. A. Alsenaidy, M. Z. Ahmad, Advances in oral drug delivery. *Front. Pharmacol.* **12**, 618411 (2021).
25. S.-H. Lee, K.-J. Kim, D.-H. Yang, K. W. Jeong, B. D. Ye, J.-S. Byeon, S.-J. Myung, S.-K. Yang, J.-H. Kim, Postpolypectomy fever, a rare adverse event of polypectomy: Nested case-control study. *Clin. Endosc.* **47**, 236–241 (2014).
26. G. P. Christophi, A. Rengarajan, M. A. Ciorba, Rectal budesonide and mesalamine formulations in active ulcerative proctosigmoiditis: Efficacy, tolerance, and treatment approach. *Clin. Exp. Gastroenterol.* **9**, 125–130 (2016).

27. D. M. Bass, M. Prevo, D. S. Waxman, Gastrointestinal safety of an extended-release, non-deformable, oral dosage form (OROS®)[1]: A retrospective study. *Drug Saf.* **25**, 1021–1033 (2002).
28. J. E. McKenzie, D. W. Osgood, Validation of a new telemetric core temperature monitor. *J. Therm. Biol.* **29**, 605–611 (2004).
29. K. Stamatopoulos, C. O'Farrell, M. Simmons, H. Batchelor, In vivo models to evaluate ingestible devices: Present status and current trends. *Adv. Drug Deliv. Rev.* **177**, 113915 (2021).

Acknowledgment: We thank V. E. Fulford (Alar Illustration) for the original artwork in Fig. 1. **Funding:** This work was funded in part by a grant from the NIH (R01EB000244), the Karl van Tassel (1925) Career Development Professorship, and the Department of Mechanical Engineering at MIT. **Author contributions:** S.S.S. and A.A. conceived and designed the RoboCap. S.S.S., A.A., A.V.H., Z.K., J.K., S.L., and N.F. performed experiments. J.K., K.I., J.J., W.A.M.M., and A.H. assisted with in vivo experimentation. R.L. and G.T. provided funding and supervised. All authors contributed to the writing of the paper. **Competing interests:** S.S.S., A.A., R.L., and G.T. are coinventors on provisional patent applications describing the developments presented here. R.L. and G.T. report receiving consulting fees from Novo Nordisk. Complete details of all relationships for profit and not for profit of G.T. can be found at the following link: www.dropbox.com/sh/szi7vnr4a2ajb56/AABs5N5i0q9AfT1IqIJAE-T5a?dl=0. Complete details for R.L. can be found at the following link: www.dropbox.com/s/yc3xqb5s8s94v7x/Rev%20Langer%20COI.pdf?dl=0. **Data and materials availability:** All data associated with this study are present in the manuscript or the Supplementary Materials.

Submitted 5 March 2022
Accepted 1 September 2022
Published 28 September 2022
10.1126/scirobotics.abp9066

Science Robotics

RoboCap: Robotic mucus-clearing capsule for enhanced drug delivery in the gastrointestinal tract

Shriya S. Srinivasan, Amro Alshareef, Alexandria V. Hwang, Ziliang Kang, Johannes Kuosmanen, Keiko Ishida, Joshua Jenkins, Sabrina Liu, Wiam Abdalla Mohammed Madani, Jochen Lennerz, Alison Hayward, Josh Morimoto, Nina Fitzgerald, Robert Langer, and Giovanni Traverso

Sci. Robot. **7** (70), eabp9066. DOI: 10.1126/scirobotics.abp9066

Science Robotics (ISSN 2470-9476) is published by the American Association for the Advancement of Science. 1200 New York Avenue NW, Washington, DC 20005. The title *Science Robotics* is a registered trademark of AAAS.